Turkish Online Journal of Qualitative Inquiry (TOJQI)
Volume 12, Issue 6, July, 2021: 8613- 8642

Research Article

CoISAE-PARCNN: Combined Improved Stacked Auto Encoder and Enhanced Pre-Activation Residual Convolutional Neural Network for the Pulmonary Nodule Detection in Lung CT and X-ray Images with robust image enhancement and segmentation techniques

K.S. Gowri Laksshmi[1]*,Dr.R. Umagandhi Phd[2]

Abstract

Lung Cancer is one among deadly disease since it is aggressive in nature as well as deferred detections at advanced stages. The survival rate due to lung cancer mainly relies on prompt detection which is regarded as major challenge. Former approaches such as iW-Net based segmentation and Enhanced Inception-Residual Convolutional Neural Network (EIRCNN) based lung nodule detection are utilized for lung cancer detection. Though traditional iW-Net architecture outperforms in an improved way for CT medical images with challenging datasets through extensive experimentations, certain aspects are lagging pertaining to architecture. Yet further examination is required for optimal features selection in Lung nodule detection. To mitigate these issues, combination of Improved Stacked Autoencoder and Enhanced Pre-Activation Residual Convolutional Neural Network (EPARCNN) is greatly utilized for pulmonary nodule detection. Also robust image enhancement in lung CT and X-ray is achieved by suggesting Fuzzy Normalized Gamma-Corrected Contrast-Limited Adaptive Histogram Equalization (FNGCCLAHE) with Nonsubsampled Contourlet Transform (NSCT) and segmentation through Sub-Intensity range-based Pulse-Coupled Neural Network (SIPCNN). LIDC-IDRI and X–ray image datasets are utilized for assessing suggested CoISAE-PARCNN system with respect to factors such as precision, recall, f-measure, Peak Signal-o-Noise Ratio (PSNR), time, error rate and accuracy. It is thereby validated through experimental outcomes that the proposed system outperforms well in contrary to various prevailing approaches like LOG, Fast-RCNN, EWRCNN and EIRCNN.

Keywords: Computed Tomography, X-ray images, Stacked Autoencoder, Enhanced Pre-Activation Residual Convolutional Neural Network, Fuzzy Normalized Gamma-Corrected Contrast-Limited Adaptive Histogram Equalization, Nonsubsampled Contourlet Transform.

1. Introduction

Lung Cancer is one among dreadful cancers across world, but preliminary stage detection may help in improving survival rate. Generally small cell growth inside the lung corresponds to Cancerous (malignant) besides noncancerous (benign) pulmonary nodules. Crucial prognosis greatly necessitates malignant lung nodules detection at a preliminary stage [1]. Differential

[1]*Research Scholar, Department of Computer Science,Kongunadu Arts and Science College, Coimbatore, Tamil Nadu.Email: gowrisasi2@gmail.com.
[2]Associate Professor and Head ,Department of Computer Technology, Kongunadu Arts and Science College, Tamil.Email:Nadu.umakongunadu@gmail.com

diagnosis is highly demanded based on minor morphological changes, locations, besides clinical biomarkers since initial phase cancerous lung nodules are desperately alike to noncancerous nodules [2]. Malignancy probability is one of the greatest challenges for detecting primary cancerous lung nodules [3]. Several diagnostic techniques like clinical backgrounds, computed tomography (CT) scan exploration (morphological assessment), positron emission tomography (PET) (metabolic assessments), and needle prick biopsy analysis are deployed by physicians for diagnosing malignant lung nodules at preliminary stage [4]. The benign and malignant lung nodules differentiation is attained by typically aggressive approaches used by healthcare practitioners like biopsies or surgeries. Since lung is a fragile and sensitive structure, there arises high risk and increased patients' anxieties. It is revealed from Globocan estimate of lung cancer that lung cancer in India is 70,275 (including all ages as well as both genders) with an age standardized incidence rate being 6.9 per 100,000 of population [5].Many research works has been carried out for CAD systems performance improvement of pulmonary nodule analysis. Conventional machine learning approaches like several gray-level thresholding, linear discriminate examination, distance transformation and Support Vector Machine (SVM)are utilized for lung nodules exploration while dealing with insufficient resources and dataset [6-7]. Conversely, Deep Learning approaches has grabbed the attention of many researchers over past ten years for medical imaging tasks. Lung nodule may vary in size, region cropping with a fixed size is not satisfactory which is mitigated by Faster R-CNN for lung nodule detection in [8]. Faster R-CNN method is modified for realizing pulmonary nodules in precise and quick manner in hundreds of two-dimensional CT chest images in addition thereby mitigating radiologist burden and achieving performance improvement of pulmonary nodule detection. Solitary pulmonary nodules are differentiated from pulmonary nodules and small nodules by this model exhibiting definite clinical impact for lung cancer early screening. Nevertheless, authenticity is a vital issue though there still ensue multiple nodule candidates created through initial rough detection in this system.CT scans Radiological heterogeneity along with lung nodules variable sizes are the greatest challenge in this research which is addressed by multi-resolution convolutional neural network (CNN) for different levels feature extraction as well as resolutions from diverse depth layers in network for lung nodule candidate's classification. Hence a robust nodule detection technique is always highly demanding for the reason of lung nodules heterogeneity as well surrounding background complexity. In [11],lung nodule detection is achieved using two-stage convolutional neural networks (TSCNN). There is no routine use of Computer-aided detection (CAD) systems by radiologists for pulmonary nodule recognition in medical practice regardless of their possible advantages. In [12], pulmonary nodules classification performance is enhanced in CT scans by suggesting a transferable texture Convolutional Neural Networks (CNN). This research integrates an Energy Layer (EL) for texture features extraction from convolutional layer by which network number of learnable parameters additionally decreases memory necessities besides computational complexity. CT scan analysis systems may succeed in huge number of false positive results in lung cancers diagnosis preliminary stage. Consequently, it is greatly necessitated for an effective and novel deep learning methodology for preliminary stage lung cancer diagnosis. Improved Stacked Autoencoder and Enhanced Pre-Activation Residual Convolutional Neural Network is greatly integrated in this research for lung pulmonary nodule recognition. The research contribution is listed below:

- A novel image enhancement technique termed as Fuzzy normalized gamma-corrected contrast-limited adaptive histogram equalization (FNGCCLAHE) with Nonsubsampled Contourlet Transform (NSCT) is introduced in this research.
- Lung CT and X-ray images Segmentation is achieved greatly by proposing a novel segmentation method called sub-intensity range based simple pulse-coupled neural network (SISPCNN).
- Feature representation learning for accomplishing recognition termed as (CoISAE-PARCNN) is presented by a novel deep learning framework which comprises Combined Improved Stacked AutoEncoder Deep Neural Network (ISAE-DNN) and Enhance Pre-Activation Residual Convolutional Neural Network (EPARCNN).
- In ISAE-DNN, three hidden layers are exploited for feature extraction followed through classification with EPARCNN at softmax classifier and feature reduction is completed by means of Intelligent Water Drop (IWD) optimization method.

The paper organization is as follows: Proposed technique along with dataset description is presented in section 2. Investigational set-up and Outcomes are compared in Section 3. Summary of Inferences and forthcoming work are provided in Section 4.

2. Proposed Methodology

Fig 1 depicts the input original image. Initially, lung nodule image contrast is enhanced by suggesting a Fuzzy Normalized Gamma-Corrected Contrast-Limited Adaptive Histogram Equalization (FNGCCLAHE) with Nonsubsampled Contourlet Transform (NSCT). High frequency noise removal is achieved using an adaptive threshold de-noising technique besides local image contrast enhancement is deployed at high-frequency sub-bands after de-noising. Over enhancement is evaded by maintaining low-frequency part deprived of being processed. Lung CT and X-ray images (as shown in Fig.1.) Segmentation is attained greatly by proposing a novel segmentation method called sub-intensity range based pulse-coupled neural network (SIPCNN). Feature representation learning for accomplishing recognition termed as (CoISAE-PARCNN) is presented by a novel deep learning framework which comprises Combined Improved Stacked Auto Encoder Deep Neural Network (ISAE-DNN) and Enhance Pre-Activation Residuel Convolutional Neural Network (EPARCNN). In ISAE-DNN, at softmax classifier three hidden layers are deployed for feature extraction subsequently classification with EPARCNN besides feature reduction is done via IWD. The Knowledge Discovery in Databases (KDD) is shown in Fig.2.

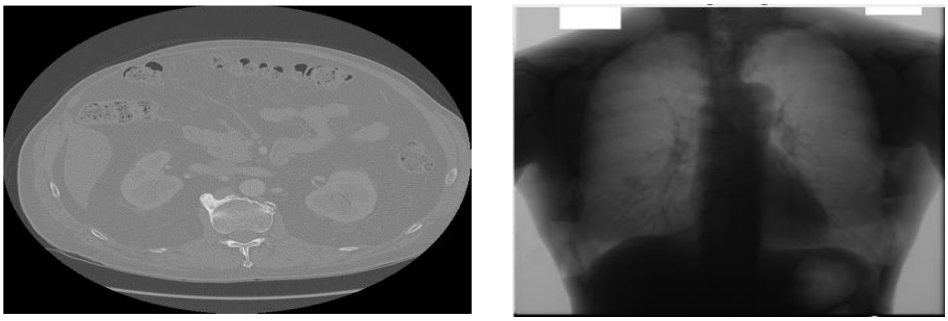

CT-image X-ray image

Fig.1. Input original image of CT and x-ray

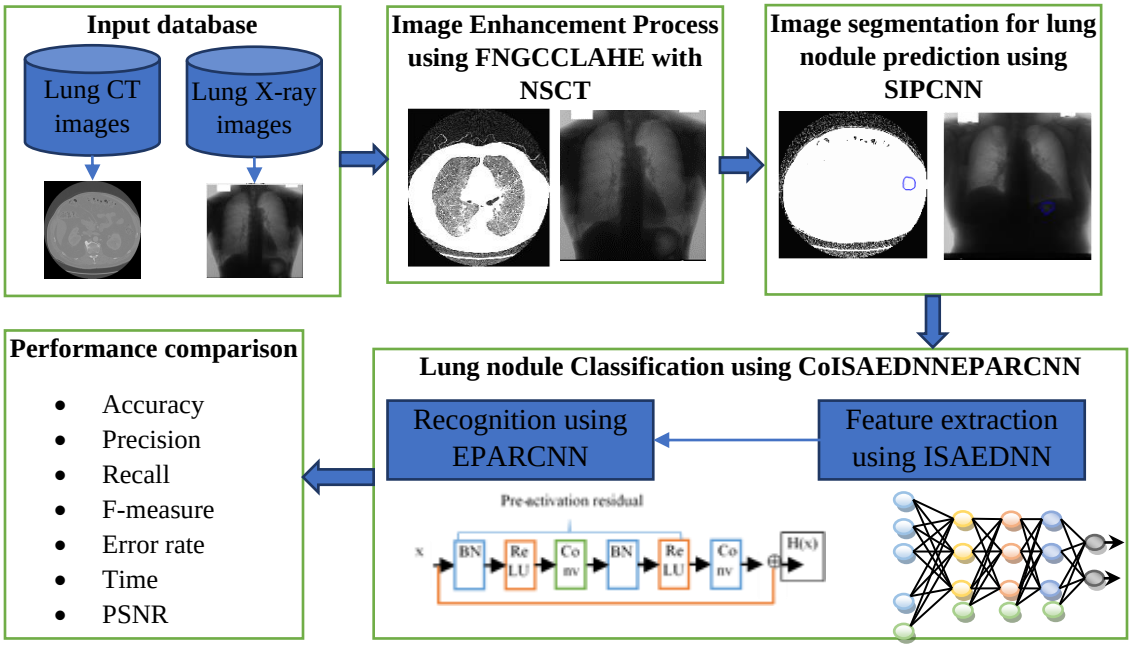

Fig 2: overall KDD diagram of proposed CoISAE-PARCNN scheme

2.1.LIDC-IDRI dataset

Lung Image Database Consortium image collection (LIDC-IDRI) dataset, which comprises of symptomatic and lung cancer screening thoracic registered tomography (CT) scans with marked-up annotated lesions and also X-ray imagesis utilized which comprises diagnostic as well as lung cancer screening thoracic computed tomography (CT) scans with marked-up annotated lesions. The CT image dataset is taken from the following link: https://wiki.cancerimagingarchive.net/display/Public/LIDC-IDRI. And the X-ray image dataset is taken from the following link: https://www.kaggle.com/hmchuong/xray-bone-shadow-supression. LIDC-IDRI is regarded as web-accessible international resource for computer-assisted diagnostic (CAD) methods expansion, training, besides assessment for lung cancer recognition and identification.

2.2.Image Enhancement

The captured images contrast of lung CT and X-ray is likely to be low, which is considered as dominant artifact reducing image quality as well as obstructs extracting its beneficial information process. Histogram-based techniques are greatly deployed for artifact processing which is a common approach. Conversely, even if, contrast enhancement can be done by these techniques for dissimilar grayscale imaging applications, outcomes are not acceptable for CT images for reason of numerous faults, noise amplification, surplus brightness, and imperfect contrast. This work taking grayscale image then contrast enhancement is done using FNGCCLAHE where NGC is used for luminance reduction. Hence, Fuzzy Normalized Gamma-Corrected Contrast-Limited Adaptive Histogram Equalization (FNGCCLAHE),an enhanced version is greatly utilized for offering improved brightness with better-quality contrast for CT images. An initial phase of a normalized gamma correction function is included for fine-tuning the processed image gamma which is regarded as the novelty part and thereby avoiding basic FNGCCLAHE common errors of excess brightness and imperfect contrast it yields.

FNGCCLAHE Method:FNGCCLAHE technique is greatly utilized for high contrast image generation when compared with original image. There are three stages in suggested fuzzy image enhancement specifically image fuzzification, membership values modification for image enhancement along with image defuzzification. The transformation of Gray level intensities to fuzzy plane is done amid 0 and 1 value range in image fuzzification. Set of fuzzy singletons in the fuzzy set notation is given by considering image f of size $M \times N$ and intensity level in range $(0, L-1)$.

And it is indicated by membership function signifying certain gray level degree. The fuzzy matrix F conforming to this lung image is articulated as

$$F = \bigcup_{i=1}^{M} \bigcup_{j=1}^{N} \frac{\mu_{ij}}{f_{ij}} \quad 0 \le \mu_{ij} \le 1 \qquad (1)$$

where f_{ij} represents intensity of $(m,n)^{\text{th}}$ pixel and its membership value. The conversion of original image f in spatial domain into fuzzy domain based on its region (i.e., dark or bright regions) is done through specific membership function. The values of above 0.5 is increased and decreasing those below 0.5 is done by reducing fuzziness of F Contrast intensification. For the reason of contrast intensification operator on fuzzy set F, alternative fuzzy set generation is done. Expression of membership function is as follows,

$$T(\mu_{ij}) = \begin{cases} 2 * (\mu_{ij})^2 & 0 \le \mu_{ij} \le 0.5 \\ 1 - \left(2 * (1 - \mu_{ij})^2\right) & 0.5 \le \mu_{ij} \le 1 \end{cases} \qquad (2)$$

Lung image enhancement is the main target of this contrast enhancement which is greatly achieved through creating bright pixel brighter as well as dark pixel darker. The middle intensity valued pixels are not altered largely. Image enhancement pertaining to its respective region occurs when image conversion into fuzzy domain membership function modification is done.

NGCCLAHE is exploited for image F fuzzy plane. Poor contrast improvement is accomplished by

CLAHE early application on low-contrast CT medical images and it can be used for clinical purposes [13]. Consequently, enhancing standard CLAHE performance is greatly desired in the meantime it has an abundant probable to be practical with present clinical routines comprising CT scans.

Proposed NGCCLAHE:

Gamma is regarded as significant property of all digital imaging system elucidating relationship amid a pixel's luminance besides its numeric value. A gray-level transformation function applied on images for their imperfect luminance enhancement is regarded as gamma correction process. Power-law transformation function is greatly utilized for achieving this [14] and appropriate for multi-purpose function contrast manipulation in spatial domain [15]. The image imperfect intensity levels are greatly corrected by using this transformation [16]. The gamma γ value alterations varies input mapping to output intensities [17]. The power-law transformation is arithmetically characterized by:

$$R = CX^{\gamma} \qquad (3)$$

where R signifies gamma-corrected image; X denotes original image, in which X pixels values lies amid 0 to 1; c is positive constant parameter controlling brightness; and γ is a positive constant parameter representing gamma value [18]. Nevertheless, parameter c is eliminated

because increasing its value may affect image details loss besides adverse brightness, which is not suggested for CT images. And so, optimized power-law P is deployed in this research, which is formulated as

$$P = X^{\gamma} \quad (4)$$

The controlling of transformation function can be done by changing gamma γ values which is main benefit of power-law transformation. But, the demerit is that increasing γ value may cause gamma image overcompensation as well as thereby darkening processed image despite the fact improving its contrast [19].

On the other hand, low-contrast images characterization is done through low-intensity dynamic range. As a result, this dynamic range expansion is greatly necessitated for fitting its full natural interval. In image processing background, dynamic range expansion also termed (normalization) is a process altering pixel intensity values range, where it is functional on images with reduced gray-level dynamic range. The term normalization is given since it takes image into a range which is quite common [20]. The subsequent normalization equation is exploited for scaling linear pixels for suitable in its full natural range:

$$N = \frac{[X - \min(X)]}{[\max(X) - \min(X)]} \quad (5)$$

Where X signifies input image, N denotes normalized image, min and max operators are utilized for getting maximum and minimum pixel values in a specified image, correspondingly. In this research, a recently established function titled Normalized Gamma Correction (NGC) is presented for exploiting gamma correction shortcoming as a crucial benefit aids in decreasing brightness as well as improving contrast while making an allowance for full dynamic range feature of normalization. The NGC equation is specified below

$$NGC = \frac{[P - \min(P)]}{[\max(P) - \min(P)]} \quad (6)$$

Lastly, NGC function inclusion to CLAHE may suggestively enhances its performance, whereas this function aids in diminishing brightness besides enhancing degraded image contrast. Henceforth, CLAHE technique is greatly used for contrast improvement as well image brightness. Consequently, adjustments are done for increasing brightness along with CLAHE unbalanced contrast for achieving an satisfactory visual superiority for processed images. The specified image contrast is enhanced by suggested NGCCLAHE in seven separate steps in Algorithm 1 and steps 2–7 have been formulated on basis of [21, 22].

Algorithm 1: NGCCLAHE

Step 1: NGC function is utilized in Equation 4 for image contrast adjustments as an initial processing phase.

Step 2: The contrast adjusted image is divided into a number of equal-sized and non-overlapping regions entitled tiles, in which it possess M × N size: This division effects in three different groups of regions. The first group is termed as corner regions (CR), comprising four corner regions. Second group is termed border regions (BR), encompassing entire border regions, excluding corner regions. Third group is so-called inner regions (IR), containing remaining image regions. For instance, if a specified image size is 512 × 512, it can be allocated into 64 regions with each possessing 8 × 8 size for decent statistical assessment attainment. Here, size of tiles is fixed to be 8 × 8.

Now, for every region, execute the succeeding:

Step 3: Obtain region local histogram: In this step, number of grayscales possessing similar value is counted for every grayscale in region. The gathering process performs these counts for all grayscales is named histogram, which is attained through cumulative distribution function (CDF). For every region, consider M and N are number of pixels, $h_{i,j}(n)$ for $n = 0, 1, 2, \dots, N - 1$ is (i, j) region histogram. Now, conforming CDF is estimated as:

$$f_{i,j}(n) = \frac{(N-1)}{M} . \sum_{k=0}^{n} h_{i,j}(k) \quad (7)$$

where $h_{i,j}(k)$ denotes pixel k histogram , and $n = 0, 1, 2, \dots, N - 1$.

Step 4: Assess clip limit value: The clip limit β can be obtained using ensuing equation:

$$\beta = \frac{M}{N}(1 + \frac{\alpha}{100}\ (S_{\max} - 1) \quad (8)$$

where α denotes clip factor and its value lie amid 0 and 100. $S_{\max}$signifies maximum allowable slope, whose value lie among 1 and $S_{\max}$.

Step 5: Clip histogram that exceeding its related clip limit: This step alters histogram on basis of acquired clip limit via limiting maximum number of counts, for every pixel to β. This can be archived by retaining histograms that are less or equal to β, whereas clipping ones that exceed β.

Step 6: Reorganize clipped histograms values to all histogram bins: A recursive uniform distribution of extra counts that exceeded clip limit is executed out between pixels with counts less than or equal to β. This once more shoves certain counts over clip limit. Consequently, resultant excess is redistributed again, and the process is repeated until clip limit is not exceeded through any counts (histogram bins) any more. Henceforth, redistribution of counts necessitates numerous iterations for every histogram.

Step 7: Compute new pixel values by mapping functions according to new histogram redistribution: Here, three mapping functions are utilized for calculating new pixel values according to their locations for contrast-limited regions. For inner regions, four nearest neighboring regions mappings are used for obtaining mapping of each region quadrant. For instance, a definite pixel in quadrant 1 of (i, j) region is mapped based on its horizontal and vertical distances from centers of $(i, j), (i, j - 1), (i - 1, j), and\ (i - 1, j - 1)$ regions. The new value estimation of pixel p in quadrant 1 of (i, j) region is given by:

$$p_{new} = \frac{s}{r+s}\left(\frac{y}{x+y} f_{i-1,j-1}(p_{old}) + \frac{x}{x+y} f_{i,j-1}(p_{old})\right) + \frac{r}{r+s}\left(\frac{y}{x+y} f_{i-1,j}(p_{old}) + \frac{x}{x+y} f_{i,j}(p_{old})\right) \quad (9)$$

Where, r, s, x, and y represents definite distances. $f_{i,j}(\cdot)$ is a cumulative distribution function. In a similar way, new pixel values for quadrants 2, 3, and 4 of (i, j) region are also assessed. For border regions, neighborhood organization is divergent. Considering this, pixel neighborhood organization which is in quadrant 1 or 3 is alike to that of inner group regions, whereas it is diverse for quadrant 2 or 4 as one such situation of quadrant 2. The new pixel p value in quadrant 2 of (i, j) region is estimated as:

$$p_{new} = \frac{s}{r+s} f_{i,j-1}(p_{old}) + \frac{r}{r+s} f_{i,j}(p_{old}) \quad (10)$$

In a similar manner, new pixel values for quadrant 4 of (i, j) region are assessed. For corner regions, diverse characteristics are perceived for dissimilar quadrants. Quadrant 4 has neighborhood organization like those of inner regions, while quadrants 2 and 3 have neighborhood organizations like those of border regions. Nevertheless, quadrant 1 is only one of its kind and there is no contact with other regions. The new value of pixel p in quadrant 1 of (i, j) region is computed as:

$$p_{new} = f_{i,j}(p_{old}) \tag{11}$$

where other corner regions mapping is done in a similar approach.

Step 8: As a final point, recently found pixel values are kept in a new array in such a way that size of which is alike to original image to obtain new improvedimage. Then contrast limited adaptive histogram equalization is applied to new enhanced image fuzzy plane F as follows

$$\bar{F} = [i_{c-max} - i_{c-min}] * F_k(i_{c-in}) + i_{c-min} \tag{12}$$

Where i_{c-min} and i_{c-max} be minimum and maximum permissible intensity levels, e optimal value of this clip limit is moreover fixed. $F_k(i_{c-in})$be cumulative distribution function (CDF) for input image i_{c-in}which is specified as

$$F_k(i_{c-in}) = \sum_{j=0}^{k} f_i(i_j) \tag{13}$$

where, probability density function is specified through

$$f_i(i_k) = \frac{n_k}{N} \tag{14}$$

Here *N* denotes total number of pixels and n_k represents number of pixels with intensity level i_k. As a final point, corresponding inverse membership functions are utilized for defuzzifying modified membership functions.

$$G(x, y) = T^{-1}\left(\bar{F}(x, y)\right) = \bigcup_{x=1}^{M} \bigcup_{y=1}^{N} \bar{F}(x, y) * (L - 1) \tag{15}$$

where, $G(x, y)$ represents $(x, y)^{th}$ pixels' gray level in enhanced image. The inverse transformation of *T* is represented as T^{-1}. It conforms to retransformation of membership values into gray-level plane.

NSCT based image denoising: NSCT is regarded as

profound development of the contourlet transform (CT) which tend to possess shift invariant characteristic. Laplacian pyramid structure is greatly utilized by CT for multi-scale image decomposition that is achieved by directional filter banks (DFBs).NSCT comprises two components: nonsubsampled pyramid structure (NSP) and nonsubsampled Directional Filter Bank (NSDFB).

NSCT helps in transformation of an image into a low-frequency lung image and: $\sum_{l=1}^{j} 2^l$, where$l$ signifies number of decomposition level, high-frequency images. These images tend to possess similar size as original image. Proper threshold selection helps in image separation of high-frequency sub-band comprising image noise. Different noise variance in both sub-band may ensue due to non-orthogonal NSCT. Correlation amid sub-bands plays a major role for maintaining more details when removing noise as well an adaptive thresholding is chosen in this research for denoising. The bayes shrink threshold is given by

$$T_b = c\frac{\sigma^2}{\sigma_x^2} \tag{16}$$

Where c denotes constant amid 0 and 1. σ^2 represents noise variance, σ_x^2 signifies signal variance

$$\sigma = \frac{median|d_{i,j}|}{0.6745} \tag{17}$$

$$\sigma_x = \sqrt{\max\left(\frac{1}{mn}\sum_{i=1}^{m}\sum_{j=1}^{n} d_{i,j}^2(1,k) - \sigma^2, 0\right)} \tag{18}$$

The coefficients average in lth levels and kth direction is presented in Eq. 19.

$$S_{1,k} = \frac{1}{m * n}\sum_{i=1}^{m}\sum_{j=1}^{n} d_{i,j} \tag{19}$$

once the decomposition level is 1, 2^1 sub-band coefficient matrices are acquired. The average is:

$$S_1 = \left(\sum_{k=1}^{n} S_{1,k}\right)/n(n = 2^1) \tag{20}$$

Weighted factors computation in different directions are given by Eq.21:

$$\lambda = S_{1,k}/S_1 \tag{21}$$

Adaptive thresholding estimation in this research is given by:

$$T = \lambda T_b \tag{22}$$

$$d'_{i,j} = \begin{cases} d_{i,j}, d_{i,j} > T \\ 0, \ \ d_{i,j} \le T \end{cases} \tag{23}$$

where, m denotes number of rows of sub-band coefficients matrix, n denotes number of columns of sub-band coefficients matrix, $d_{i,j}$ notates coefficient at (i,j) and $d'_{i,j}$ represents coefficient after lung image de-noising.

2.3.Image segmentation using SIPCNN

Computational complexity is chiefly simplified through modulating internal activity and dynamic threshold which is achieved by novel PCNN image processing methods. It also obtains sub-intensity ranges for both segments through empirical or automatic parameter values.

Yang et al. [23] suggested a new heterogeneous simplified pulse coupled neural network (HSPCNN) model via three diverse SPCNN cells with diverse structures besides parameters. This approach is regarded as simple way for testing images segmentation into numerous regions based on their gray intensities. Automatic fixing of model parameters is done by simplified PCNN characteristics. The simple model PCNN is an artificial neural network possessing only a single layer besides no training is necessitated. The relation amid network neurons as well as image pixels is a one-to-one correspondence. In contradiction of other PCNN models, Chen et al.'s SPCNN model [24] resultant from Zhan et al.'s spiking cortical model (SCM) model [30] shows a substantial part for image segmentation in addition its dynamical equations expression is given by:

$$F_{ij}[n] = S_{ij} \tag{24}$$

$$L_{ij}[n] = V_L \sum_{kl} W_{ijkl} Y_{kl}[n-1] \tag{25}$$

$$U_{ij}[n] = e^{-\alpha_f} U_{ij}[n-1] + S_{ij}\left(1 + \beta V_L \sum_{kl} W_{ijkl} Y_{kl}[n-1]\right) \tag{26}$$

$$Y_{ij}[n] = \begin{cases} 1, & if\ U_{ij}[n] > E_{ij}[n-1] \\ 0, & else \end{cases} \quad (27)$$

$$E_{ij}[n] = e^{-\alpha_e} E_{ij}[n-1] + V_E Y_{ij}[n] \quad (28)$$

Where $W_{ijkl} = \begin{bmatrix} 0.5 & 1 & 0.5 \\ 1 & 0 & 1 \\ 0.5 & 1 & 0.5 \end{bmatrix}$ (29)

$$\alpha_f = \log\left(\frac{1}{\sigma(S)}\right) \quad (30)$$

$$\beta = \frac{\left(\frac{S_{max}}{S'}\right) - 1}{6V_L} \quad (31)$$

$$V_E = e^{-\alpha f} + 1 + 6\beta V_L, V_L = 1 \quad (32)$$

$$\alpha_e = \ln\left(\frac{\frac{V_E}{S'}}{\frac{1-e^{-3\alpha_f}}{1-e^{-\alpha_f}} + 6\beta V_L e^{-\alpha_f}}\right) \quad (33)$$

In case of SPCNN, Neuron N_{ij} in position (i, j) comprises two inputs: basic feeding input $F_{ij}[n]$, representing an input stimulus S_{ij}, linking input $L_{ij}[n]$, representing eight neighboring outputsproducts, synaptic weight W_{ijkl}as well as a weighing factor V_L. S_{ij} denotes original images normalized pixel intensities. Above inputs modulations are done by linking strength β to obtain an internal activity $U_{ij}[n]$. It mainly comprises former internal activity modulated via decay factor$e^{-\alpha_f}$. At this point, if internal activity $U_{ij}[n]$ is more than dynamic threshold $E_{ij}[n-1]$, neuron N_{ij}might fire $(Y_{ij}[n] = 1)$ as well as dynamic threshold abruptly rises by a weighing factor VE. Whenever internal activity $U_{ij}[n]$ is less than dynamic threshold $E_{ij}[n-1]$, $(Y_{ij}[n] = 0)$is not fired by neuron N_{ij}, dynamic threshold might fall via decay factor $e^{-\alpha_e}$. $\alpha_f$and $\alpha_e$denote internal activity $U_{ij}[n]$ and dynamic threshold $E_{ij}[n]$ decay factors of respectively. More precisely, SPCNN comprises five significant parameters β, α_f, α_e, V_L, V_E. These parameters can be fixed in an automatic way for object segmentation in multifaceted prospects.

Image segmentation by using improved Sub-intensity range in SPCNN model: The simple pulse coupled neural network (SPCNN) dynamic properties can be clearly realized through final segmentation outcomes necessitating four iterations contained by first effective pulse cycle. SPCNN contains finite segmentation phases considerably when compared to preceding PCNN models in addition appropriate thresholds can be selected in automatic way for attaining regions segmentation at every iteration.

The medical images using SPCNN helps in fragmenting object and background regions in third iteration as well as form segments in subsequent iterations additionally. Nonetheless, it yet necessitates for calculation of five key parameters besides definitely creates bad segmentation outcomes, specifically in high intensity regions. Consequently, a SIPCNN model is suggested for further computational complexity reduction as well enhancing image segmentation precision. SIPCNN model changes SPCNN five key parameters to three. Hence parameters combination αf and αe yield one parameter α, and parameter V_L is eliminated on the basis of a Parameter-Adaptive (PA) -PCNN known as PA-PCNN[25]. Parameter β only has a fine modification via comparing with SPCNN equation, parameter$V_E$is altered to parameter V. The above three

adjusted parameters only comprises a known variable S', denoting normalized Otsu thresholding.

Parameter α

α_f and α_e signify SPCNN internal activity and dynamic threshold decay factors , correspondingly. The above two parameters combination in SIPCNN yields one parameter α and its expression given by

$$\alpha = \alpha_e = \alpha_f = \log\left(\frac{1}{S'}\right) \tag{34}$$

In (33), parameter S represents normalized OTSU thresholding. The distribution ranges of S' and α are $1 \geq S' > 0$ and $+\infty > \alpha \geq 0$, respectively. Evidently parameter α increases with decrease in parameter S'.

Parameter β

To profoundly realise neuron firing settings, constant synaptic weight W_{ijkl} in (29) is reset as well as parameter β in (31), respectively. In SIPCNN, every neuron might get affected from its four neighboring neurons instead of eight in SPCNN, parameter W_{ijkl} is also rewritten as

$$W_{ijkl} = \begin{bmatrix} 0 & 1 & 0 \\ 1 & 0 & 1 \\ 0 & 1 & 0 \end{bmatrix} \tag{35}$$

In contradiction of SPCNN, constant synaptic weight W_{ijkl} in SIPCNN is converted to four neighboring neurons sooner than eight by reason of lower computational complexity and smoother segmented contour for medical images. Since $S_{max} \approx 1$ in utmost images and $V_L = 1$ in (32), β value is reset as

$$\beta = \frac{1 - S'}{4S'} \tag{36}$$

Parameter v

βV_L would be an overall factor, conforming to (26). Simultaneously, parameter VL valuein (10) is 1. Hence, parameter V_L can be eliminated, and linking input expression is reformulated as follows,

$$L_{ij}[n] = \beta \sum_{kl} W_{ijkl} Y_{kl}[n-1] \tag{37}$$

In SPCNN, V_E can be reset as V by solely involving the normalized Otsu thresholding S' since the parameter V_E possesses a high computational complexity. Chen et al. [7] mathematical expression might be adopted as follows,

$$\begin{cases} Us_{high}[1+l] \leq E[1+l-1] \\ Us_{low}[1+l+1] > E[1+l] \end{cases} \tag{38}$$

In accordance with (37), internal activity highest value for unfired pixels in $(1 + l)^{th}$ iteration would be lower than dynamic threshold $E[1 + l - 1]$ in $(1 + l - 1)$th iteration, conversely least value of internal activity for fired pixels in $(1 + l + 1)$th iteration would be greater than dynamic threshold $E[1 + l]$ in the $(1 + l)$th iteration. Through this, the existence of a sub-intensity range of firing pixels in the (1 + l + 1)th iteration is assured. As a result, $Y[0], U[0]\ and\ E[0]$initial values are fixed to 0. Instead of third iteration, if a normal image attains first segment in SPCNN second iteration, parameter l can be set as 0. Consequently, the firing neurons converge the criterion.

$$\begin{cases} U_{high}[1] \leq E[0] \\ U_{low}[2] > E[1] \end{cases} \tag{39}$$

Nevertheless, under normal scenarios, $U[1]$ is greater than 0 and $E[0]$ is set to 0. This conforms first firing condition in (38). Consequently, the firing condition in (38) can be reset as follows, for acquiring the first image segment in second iteration.

$$U_{low}[2] > E[1] \tag{40}$$

With regard to (26), (34), (35) and (36), $U_{low}[2]$ can be formulated as,

$$U_{low}[2] - S_{low}(1 + e^{-\alpha} + 4\beta) = S_{low}M[2] \tag{41}$$

In accordance with (28) and (34), E[1] = V. Hence the Eq. (41) can be reformulated as follows

$$S_{low}M[2] > V \tag{42}$$

Further, the normalized Otsu thresholding S' that always produce a higher value than S_{low} is replaced by (43) as follows

$$S'M[2] > V \tag{43}$$

Additionally, V unique value is attained in light of maximum limiting in (43)

$$V = S'M[2] \tag{44}$$

In accordance with (36), (41) and (44), parameter V is simplified as

$$V = 1 + S'^2 \tag{45}$$

Subsequently, a small offset $(-S'^8)$ can be added further for enhancing the precision of image segmentation. Eventually, parameter V is expressed as follows,

$$V = 1 + S'^2 - S'^8 \tag{46}$$

SPCNN and SIPCNN possess the similar expressions in the fundamental model, but they differ in terms of parameter setting procedures. In the SPCNN, Eqs. (24)–(28) remain unchanged, whereas Eqs. (29)–(33) is reformed to Eqs. (30)–(32), and (24) in MSPCNN. Consequently, the SIPCNN consists of Eqs. (1)–(5) on the basis of fundamental model, and Eqs. (12)–(14), and (46) from key setting parameters. Post-segmentation of lung image, the image is processed through feature extraction using ISAE-DNN.

2.4.Feature extraction by using ISAE-DNN

For lung nodule classification, this research study proposes the model that is based on Deep Neural Network using Improved Stacked Auto-Encoders (ISAE-DNN), since this work significantly engrossed by the valuable features of deep networks, as regards enhancing each evaluation metric of the classification issue. The Improved Stacked Auto-encoders accompanied by three hidden layer of feature extraction process and the softmax layer has employed to construct DNN classifier for lung dataset. To implement classification task, the softmax layer is attached to the final hidden layer. For the provided record, nodule class and non-nodule class probabilities are given by the output layer.

Assume that ISAE network includes three layers, where the raw input is notated by I, the reconstruction of image is signified by I', and the weights and bias terms for the lth layer encoder and decoder are denoted by $\omega^{(l,1)}, \omega'^{(l,1)}, b^{(l,1)}, b'^{(l,1)}$, correspondingly, i.e.$l = 1, 2, 3$. As expressed in Eq. (47), initially ISAE maps input image into a hidden representation $h(l)$.

$$h_i^{(l)} = f\left(I'^{(l)}_i\right) \tag{47}$$

$$f\left(I'^{(l)}_i\right) = s_f\left(\omega^{(l,1)} I'^{(l)}_i + b^{(l,1)}\right)$$

Subsequently, as defined in Eq. (48), the latent representation $h(l)$ mapped back into a reconstruction $\Re$ from a corrupted version I' as follows,

$$r = g\left(h_i^{(l)}\right) \quad (48)$$
$$g(I^l) = s_g\left(\omega'^{(l,1)}h^l + b'^{(l,1)}\right)$$

in which, nonlinear activation function is defined as $s_f$and s_g. The reconstruction error $\Re e(I', \Re)$ between original input I' and reconstruction $\Re$ represents the cost function for Stacked Auto-Encoders (SAE),which can be expressed as,

$$J_{SAE} = \sum_{l=1,2,3} \Re e\left(I'^{(l)}, g\left(f\left(I_i'^{(l)}\right)\right)\right) \quad (49)$$

Here, $\Re e(I', \Re) = \|I' - \Re\|^2$. Besides, hidden units of SAE have added with a sparsity constraints term ρ, and the objective function in Eq. (50) has presented with an additional penalty terms I. Consequently, the new cost function of ISAE can be revised as,

$$J_{MSAE}(\theta) = J_{SAE} + \chi \sum_{j=1\ to\ m} KL(\rho \parallel \rho_j) \quad (50)$$

The cross-entropy within ρ and ρ_j represents the additional penalty terms Kullback–Leibler divergence (KL) expressed in Eq. (6).

$$KL(\rho \parallel \rho_j) = \sum_{j=1}^{m} \rho \log \frac{\rho}{\rho_j} + (1-\rho) \log \frac{1-\rho}{1-\rho_j}, \rho_j = \frac{1}{k}\sum_{i=1}^{k} h_i \quad (51)$$

In which, the target sparsity level for the *j*th unit is signified by ρ_j; the average activation rate is denoted by ρ_j; the number of hidden units is represented by m; and the weight for penalty terms is indicated by χ. Through identifying a set of over complete base vectors, the input data is represented, for which the sparsity dictionary encode is employed in all layers as regards attaining the optimal feature of image. Since the sparse feature representation created at the pixel level, the essential feature of an image is learned through the three hidden layer sparse coding approach [31]. Through cascading stacked auto-encoder using softmax classifier, the deep network classifier is created, during which the stacked auto-encoder may include two or more than two auto-encoders layers. The DNN classifier with ISAE includes three auto-encoders, which is depicted in Fig. 2. Consider the input vector fed into DNN as an input as $\{I_1, \dots, I_n\}$, variables as $\{Y_1, \dots, Y_n\}$ and the corresponding output class. Specified training input image vectors, training approach tends to modify DNN parameters, as regards learning input vectors, and classifying respective output value accompanied by maximum accuracy. The following steps define method for the training of ISAE-DNN classifier.

1. At first, the first autoencoder layer is trained with original input vector $\{I_1, \dots, I_n\}$ with identical as target vector. This layer efforts for input reconstruction through deriving features $\{c_{(1,1)}, \dots, c_{(1,C)}\}$ with the structure of autoencoder.
2. The second autoencoder layer training is done by considering output vector as input vector and generates output vector of first autoencoder layer $\{c_{(1,1)}, \dots, c_{(1,C)}\}$ as input vector and generates output vector $\{c_{(2,1)}, \dots, c_{(2,R)}\}$. Second autoencoder layer efforts to reconstruct input $c_{(1,C)}; i = 1,2, \dots, C$.

3. The third autoencoder layer is trained by considering the output vector as input vector and generates output vector of the second autoencoder layer $\{c_{(2,1)}, \dots, c_{(2,R)}\}$ as input vector and generates output vector $\{c_{(3,1)}, \dots, c_{(3,U)}\}$. The third autoencoder layer efforts for input reconstruction$c_{(2,i)}; i = 1,2, \dots, R$.
4. The stacked autoencoder is cascaded with softmax classifier layer. This layer is trained by considering third autoencoder layer's output, $c_{(3,i)}; i = 1,2, \dots, U$ as input vector and original class variables $\{Y_{(1)}, \dots, Y_{(N)}\}$ being target vector that is attained from training data.
5. Ultimately, back propagation is applied for enhancing the efficiency of the DNN in terms of feature extraction, which is represented as fine tuning. Through retraing of the network alongside training data, this fine tuning is carried out in a supervised approach. Post-processing feature extraction and reduction, EPARCNN is exploited to classify the features.

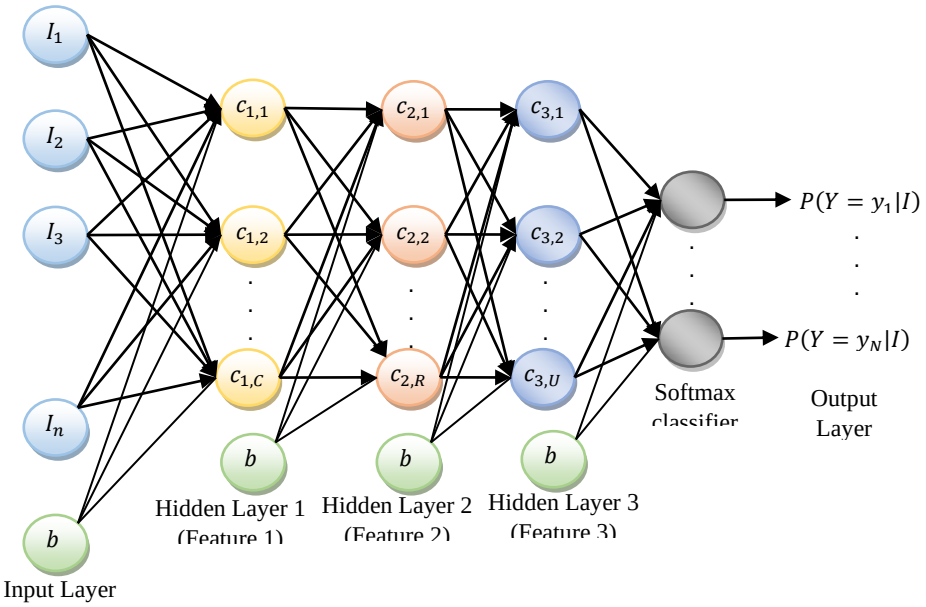

Fig.2.ISAE-DNN model

2.5.Feature selection using IWD

IWD based feature selection algorithm [29] is implemented to select best features to provide an accurate and fast classification. The IWD algorithm constructs an optimal solution through cooperation among a group of agents called water drops. The algorithm imitates the phenomena of a swarm of water drops flowing with soil along a river bed. Procedurally, each water drop incrementally constructs a solution through a series of iterative transitions from one node to the next until a complete solution is obtained. Water drops communicate with each other through an attribute called soil, which is associated with the path between any two points. The soil value is used to determine the direction of movement from the current node to the next, whereby a path with a lower amount of soil is likely to be followed as shown in Fig.3.

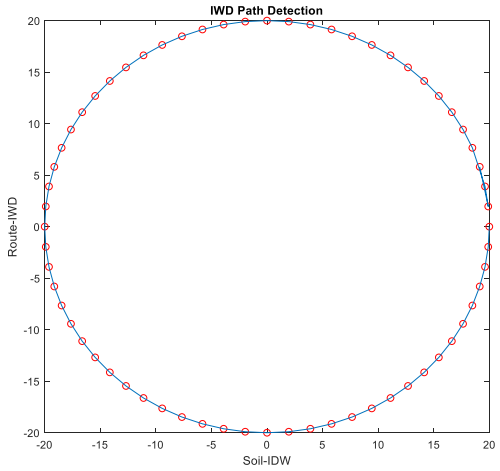

Fig.3. IWD path detection

First, we construct a graph from our features to use IWD algorithms and then we set the initial soil $(Soil_{init})$ of features, initial velocity of water drops (Vel_{init}), number of water drops (N_{IWD}), soil updating parameters $(a_{soil}, b_{soil}, c_{soil}, \rho)$, and velocity updating parameters $(a_{vel}, b_{vel}, c_{vel})$are some constant velocity parameters that are set for the given problem. After initialization the parameters, for each IWD, here choose n (distinct) features (f). Herecompute the probability $Prob(i)$ according to (52). At the beginning, water drops are spread randomly at the nodes of the construction graph, and visited nodes list $(F)$is updated to include the start node

$$Prob(i) = \frac{fitness(soil(i))}{\sum_{k \notin F} f(soil(k))} \qquad (52)$$

where $Prob(i)$ represents the probability of selecting node i, $fitness(soil(i))$ is the fitness function. The fitness function of candidate node i is inversely proportional to the absolute soil value

$$fitness(soil(i)) = \frac{1}{\varepsilon_{small} + g(soil(i))} \qquad (53)$$

where ε_{small} is a small positive number, $g(soil(i))$ used to prevent the division by zero in function $fitness(soil(i))$which is calculated as follows:

$$g(soil(i)) = \begin{cases} soil(i) & if \min_{k \notin F}(soil(k)) \geq 0 \\ soil(i) - \min_{k \notin F}(soil(k)) & otherwise \end{cases} \qquad (54)$$

where $soil(i)$ refers to the amount of soil within the node (feature) i and $soil(k)$ refers to the amount of soil within the node k which is not selected before. Then, add the newly selected node i to the feature list F. The $min()$ function returns the minimum value of its arguments. After selecting n features according to (52), the training dataset is classified by using the selected features and the F-score value which is a real number in range $[0, 1]$, of the classification is taken to measure the "quality" of the selected features. If the computed F-measure is high, this means

that the selected features are valuable. Then, F-measure value is used to update the velocity and the soil values. For each IWD, the velocityIWD_{vel} is updated as follows

$$IWD_{vel}(t+1) = \frac{IWD_{vel}(t)+a_{vel}}{b_{vel}+c_{vel}\times\sum_{i\in F} soil(i)} \quad (55)$$

where $a_{vel}, b_{vel}, c_{vel}$ are the static parameters used to represent the nonlinear relationship between the velocity of water drop IWD, i.e.IWD_{vel}, and the inverse of the amount of soil in the local node, i.e. $soil(i)$. The amount of soil$\Delta soil(F)$ that the IWD loads from the selected features is

$$\Delta soil(F) = \frac{a_{soil}}{b_{soil}+c_{soil}\times time^2\left(F, IWD_{vel}(t+1)\right)} \quad (56)$$

Where$time^2\left(F, IWD_{vel}(t+1)\right)$time taken for an IWD having the velocity$IWD_{vel}(t+1)$ to move from the current node i to next node j is calculated by

$$time^2\left(F, IWD_{vel}(t+1)\right) = \frac{1}{F-measure(F)\times IWD_{vel}(t+1)} \quad (57)$$

here F refers to the selected subset of features and F-measure(F) refers to the F-measure value of the selected features. The IWD's soil, IWD_{soil}, is increased by removing some soil of the selected features F. Update the soil of the IWD as

$$IWD_{soil} = IWD_{soil} + \Delta soil(F)$$

The soil values of all features are updated as follows

$$soil(i) = \begin{cases} (1-\rho)\times soil(i) - 2\rho\times\Delta soil(F), & if\ i\in F\ and\ F\ is\ best \\ (1-\rho)\times soil(i) - \rho\times\Delta soil(F), & if\ i\in F\ and\ F\ is\ not\ best \\ soil(i), & if\ i\notin F \end{cases} \quad (58)$$

The above computations are repeated for each IWD and the best feature set is recorded. All these processes continue until the termination condition is met. Post-selection of features, they have classified as lung cancer region deprived of utilizing EPARCNN classifier. The algorithm of IWD based feature selection are described in pseudo code given below:

Table.1. Pseudo code of IWD based feature selection algorithm.

Input: Training samples of lung images and Nset of all features
Output: set of best n features
1. Initialize the static parameters i.e. parameters are not changed during the search process.
2. While algorithm termination condition is not met do
3. Initialize the dynamic parameters i.e. parameters changed during the search

process.
4. Spread N_{IWD} number of water drops randomly on a construction graph.
5. For each IWD do
6. Choose n features by using roulette wheel that is formed according to the probabilities of features that are computed with respect to soil values of features.
7. Classify documents by using selected n features and compute the F-measure.
8. By using the computed F-measure value, update the soil and velocity values of the IWD, and the soil value of all features in the feature space.
9. end
10. Choose the best feature set found so far.
11. Until the termination condition is met.
12. Return the best feature set.

2.6.Enhanced Pre-Activation Residual Convolutional Neural Network (EPARCNN)

The EPARCNN framework significantly tends to enhance the efficiency of recognition process through utilizing same/less number of computational metrics, when compared to similar kind of deep learning methods. The proposed EPARCNN method adopts the residual block as the vital element, which is represented in Fig 3(a). Accordingly, there are two convolutional layers besides a residual connection (skip connection) comprised in residual block. This skip connection additionally aggregates low-level, and high-level features. Thus, the gradient vanishing or explosion problem occurs in deep network can get reduced through the residual block. The estimation of each residual can be formulated as,

$$H(x) = f(F(x) + x) \qquad (59)$$

Here, residual block's input and output is represented by x and $H(\cdot)$, respectively. A residual learning function is denoted by F;the convolutional layer output is represented by $F(x)$ that is prior to summation operation; and the activation function is indicated by f .

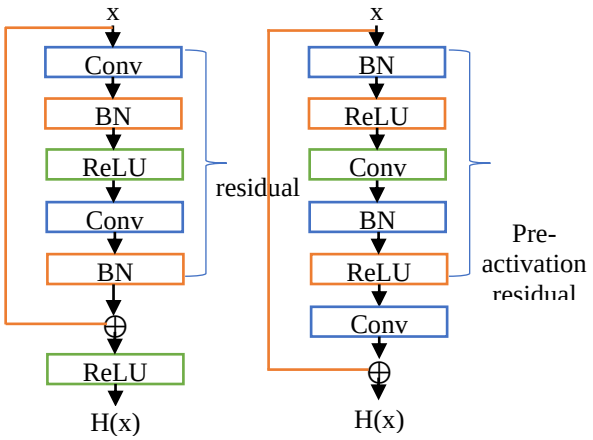

Fig 3. Normal residual block (a) and Pre-activation residual block (b)Architecture.

Here, in the suggested network's residual block, the Batch Normalization (BN) and pre-activation mechanism have applied for attaining the optimal performance. The implementation of pre-activation architecture is carried out by means of shifting BN and rectified linear units (ReLU) activation function prior to convolution operation as depicted in Fig 4(b). The formulation of pre-activation residual block is expressed as

$$H(x) = F(x) + x \qquad (60)$$

Fig 4(a) demonstrates that activation function f in (1) is ReLU, can be formulated as follows

$$f(x) = \max(0, x) \qquad (61)$$

If the signal is negative, the signal is forcibly converted to 0 by the ReLU, through which a few useful residual features from normal residual block may be lost. Consider the f as an identity mapping, then (1) will be the same value of (2). Through identity mapping, signals can get enabled to being directly propagated within any two units, which ensures that features learned by residual learning function have prevented from loss. Thus, the process of network training is simplified by the pre-activation mechanism, besides the network generalization performance is improved.

EPARCNN block is considered being the highly substantial element of this proposed architecture, in which residual units, inception units, and RCLs have involved. The process of this architecture can be described as follows, i) the inputs are fed into input layer, ii) passed through inception units, where RCLs are applied, iii) inception units output are added to IRRCNN-block input. According to various sized kernels in inception unit, the recurrent convolution operations implement. The prior time step outputsis added with the output at the current time step, since because of the recurrent structure inside convolution layer. Subsequently, outputs at present time step is considered as input for following time step. With regard to considered time steps, the same operations are executed. For instance, EPARCNN-block comprises 3 RCLs which is characterized by k=2, in which the dimensions of the input and output remain unchanged. It is merely considered as an accumulation of feature maps pertaining to time steps. Consequently, through equal number ofnetwork parameters the optimal recognition accuracy is obtained, which has ensured by the robust features. In accordance with the discrete time steps, the RCL operations have carried out, besides they have articulated based on RCN [26]. Assume that the xl input sample located in the EPARCNN-block's lth layer and a pixel located at (i, j) in an input sample on the kth feature map in the RCL. Besides, consider that network $O_{ijk}^{l}(t)$output is at time step t. Then, output is formulated as,

$$O_{ijk}^{l}(t) = \left(w_k^f\right)^T * x_l^{f(i,j)}(t) + (w_k^r)^T(t-1) + b_k \qquad (62)$$

In which, the standard convolution layers has fed with $x_l^{f(i,j)}$and l^{th} RCL has fed with $(w_k^r)^T(t-1)$ as an inputs. The values of $w_k^f$and w_k^r have considered being the typical convolutional layer and RCL of kth feature map, correspondingly. Whereas, bk represents the bias.

$$y = f\left(O_{ijk}^{l}(t)\right) = \max\left(0, O_{ijk}^{l}(t)\right) \qquad (63)$$

In the above equation, the standard Rectified Linear Unit (ReLU) activation function is signified by *f*. Besides, the performance of this framework has determined using Exponential Linear Unit (ELU) activation function in the subsequent experiments, in which $y_{1x1}\ (x), y_{3x3}\ (x), \text{and} y_{1x1}^{p}\ (x)$ indicate outputs y of inception units for various size kernels and average pooling layer, correspondingly. And, $\mathcal{F}(x_l\ , w_l)$ is the formulation of the final outputs of EPARCNN unit, which can be estimated as follows,

$$\mathcal{F}(x_l\ , w_l) = y_{1x1}\ (x) \odot \text{y(x)} \odot y_{1x1}^{p}\ (x) \tag{64}$$

Where, $\odot$ signifies the concatenation operation as regards the channel/feature map axis. Further, RCNN-unit outputs are added to the inputs of EPARCNN-block. The subsequent equation expresses the EPARCNN-block's residual operation.

$$x_{l+1} = x_l + \mathcal{F}(xl\ , wl) \tag{65}$$

Here, the inputs for the instantaneous next transition block is defined as x_{l+1}, the EPARCNN - block's input samples is indicated by x_l, the l th EPARCNN-block's kernel weights is signified by wl, and the outputs from of l th layer of the EPARCNN-unit is denoted by $\mathcal{F}(x_l\ , w_l)$. As represented in the EPARCNN-block depicted in Figure 3, the number of feature maps are equal to dimensions of feature maps for residual units. Eventually, EPARCNN-block outputs is being applied with batch normalization.

As inspired by NiN [27] and Squeeze Net [28] models, solely 1×1 and 3×3 convolution filters are used during this implementation. Besides, it supports to retain the minimum number of network parameters. Through adding a 1×1 filter the non-linearity of decision function can get increased deprived of influencing the convolution layer. The input and output features size is simply a linear projection on same dimension, since it remains unchanged in the IRRCNN blocks, besides non-linearity is added to RELU and ELU activation functions. Following each convolution layer in transition block, 0.5 dropout is utilized. Ultimately, at the end of the architecture, a Softmax, or normalized exponential function layer is utilized. For input sample x, weight vector W, and K distinct linear functions, Softmax operation can be defined for ith class as follows:

$$P(y = i|x) = \frac{e^{x^T} w_i}{\sum_{k=1}^{K} e^{x^T} w_k} \tag{66}$$

In order to evaluate assess the proposed EPARCNN framework, a set of experiments have done on various benchmark datasets and obtained outcomes are related over various models. The framework of proposed EPARCNN is shown in Fig.5.

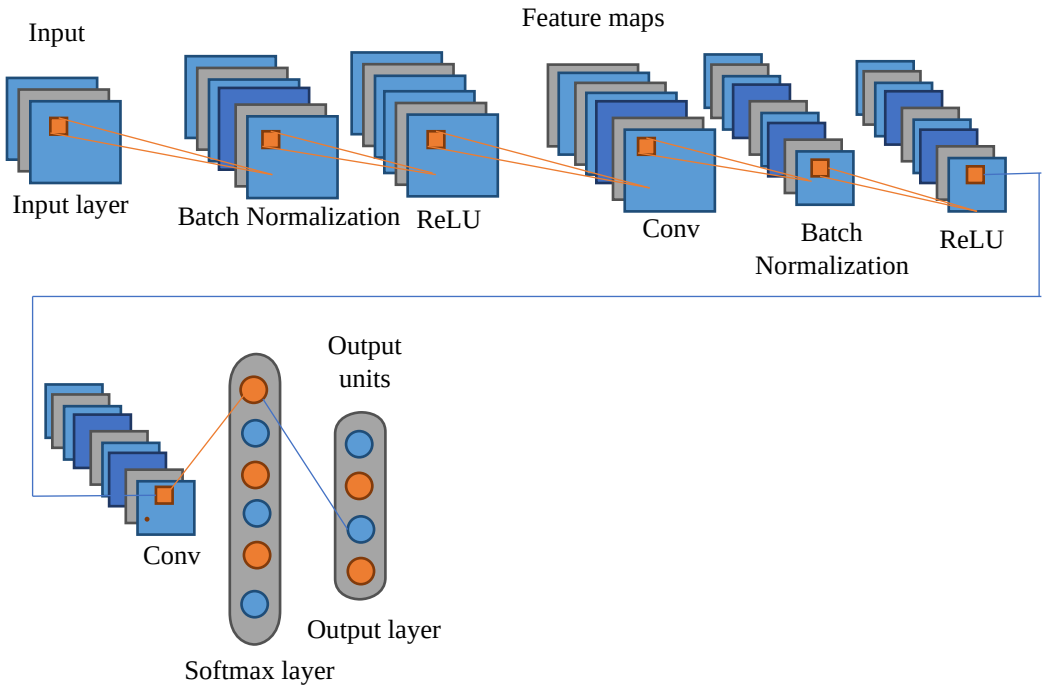

Fig.5. The framework of EPARCNN method

3. Experimental Results and discussion

In this segment, the performance evaluation is carried out for the proposed CoISAE-PARCNN approach. Besides, the results have compared with the prevailing lung nodule detection methodologies, like LOG, Fast-RCNN, EWRCNNandEIRCNN. The real-time Lung Image Database Consortium image collection (LIDC-IDRI) includes diagnostic and lung cancer screening thoracic lung CT and X-ray scans accompanied by marked-up annotated lesions. This data set has jointly created by eight medical imaging organizations and seven academic centers, in which 1018 cases have included. The images from clinical thoracic CT scan and an associated XML file have included that archives two-phase image annotation process outcomes, which has accomplished by four proficient thoracic radiologists. The subsequent figures clearly depict the efficiency of the proposed approach to deliver optimal performance as regards the performance metrics, such as accuracy, precision, recall, f-measure, error rate, time and PSNR. In Table 1 and Table 2, the numerical outcomes of CT images and X-ray images for the proposed CoISAE-PARCNN, as well as the prevailing LOG, Fast-RCNN, EWRCNNandEIRCNN methods have listed out.

Table 1: Performance evaluation metrics for CT images

Performance Evaluation metrics	Existing LOG	Existing Fast-RCNN	Proposed EWRCNN Phase 1	Proposed EIRCNN Phase 2	Proposed CoISAE-PARCNN Phase 3
Accuracy	81.73	87.16	93.86	94.05	98.25

Precision	52.99	54.57	59.38	59.70	83.09
Recall	81.40	87.10	93.76	95.32	98.19
F-measure	64.19	67.10	70.71	73.12	90.01
Error rate	19.36	12.83	7.13	5.94	1.74
Time	3.30	2.89	2.10	1.92	1.63
PSNR	41	42	44	46	47

Table 2: Performance evaluation metrics for X-ray images

Performance Evaluation metrics	**Existing LOG**	**Existing Fast-RCNN**	**Proposed EWRCNN Phase 1**	**Proposed EIRCNN Phase 2**	**Proposed CoISAE-PARCNN Phase 3**
Accuracy	81.73	87.72	92.50	93.64	98.60
Precision	50.87	51.46	52.48	53.96	73.55
Recall	81.14	88.16	92.57	94.90	98.49
F-measure	63.53	64.99	66.99	70.72	85.88
Error rate	19.26	12.27	8.49	6.35	1.39
Time	4.5	3.19	2.36	2.11	1.98
PSNR	39	40	43	44	45

3.1.Precision Result comparison

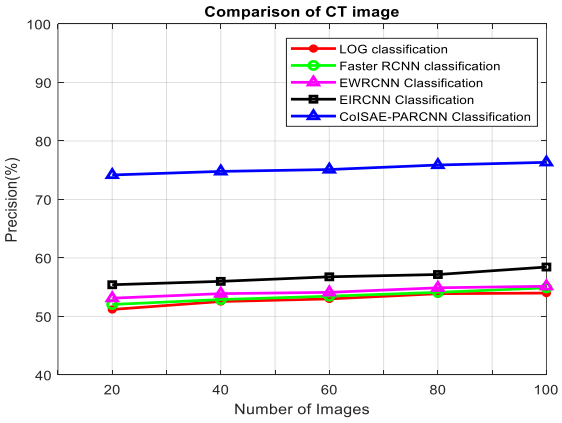

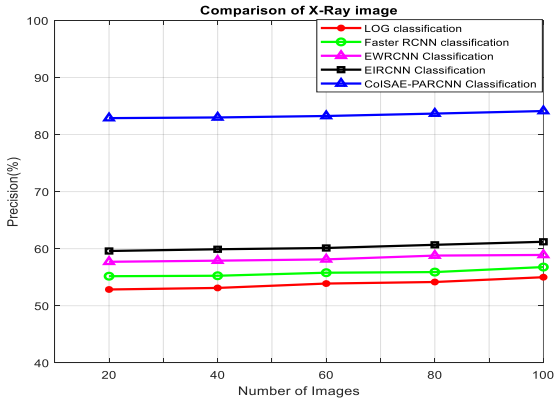

Fig.4. Precision performance comparison in several compression techniques

In Fig. 4, precision outcomes obtained by proposed CoISAE-PARCNN, and existing LOG, Fast-RCNN, EWRCNN and EIRCNN methods have compared. From the graphs, the proposed approach proves to be efficient than other prevailing methods as they represent that the proposed CoISAE-PARCNN approach precisely obtains the lung nodule, i.e.83.09% and 73.55% of the precision rate for CT and X-ray respectively, which is superior to other existing methods. Moreover, the results depict that the proposed technique is efficient than prevailing methods in terms of image enhancement using FNGCCLAHE with NSCT that that mean brightness can be achieved as the original mean brightness is retained and thus the proposed method has been found effective in enhancing contrast of images in comparison to few existing methods and further attained high precision rate.

3.2.F-measure Result Comparison

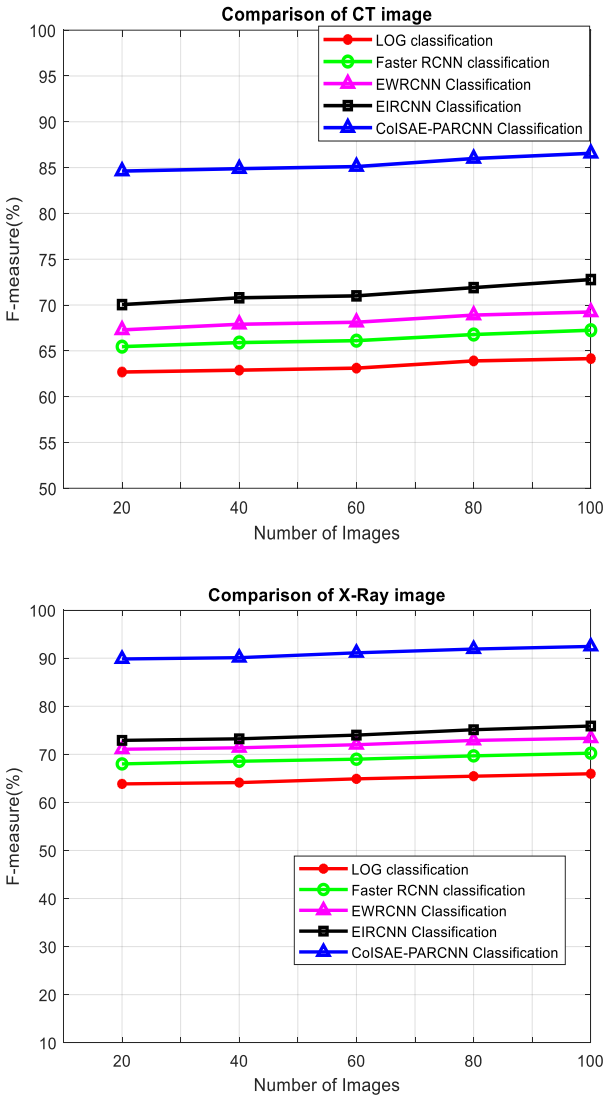

Fig.5. F-measure performance comparison in several compression techniques

Fig. 5 compares proposed CoISAE-PARCNN, and existing LOG, Fast-RCNN, EWRCNN and EIRCNNmethodF-measure values. The graphs depict the proficiency of the proposed approach to secure 90.01% and 85.88%of F-Measure for CT and X-ray respectively, which signifies that it is optimal in lung nodule detection, and is superior to other prevailing approaches. The reason is that proposed CoISAE-PARCNN technique performs on the basis of appropriate feature extraction and feature selection methods. Whereas, low rate of F-Measure values has attained for both x-ray and CT images by the prevailing methods, like RCNN, Faster RCNN, EIRCNN and EWRCNN, correspondingly. Thus, the proposed technique is proved to be efficient than other prevailing approaches as regards lung nodule detection.The reason is that,the feature space is reduced by IWD technique having advantage of in-place computation and thus reduce the computational complexity of the proposed system and enhancing the performance of learning algorithm of EPARCNN and thus produce high f-measure results.

3.3.Recall Result Comparison

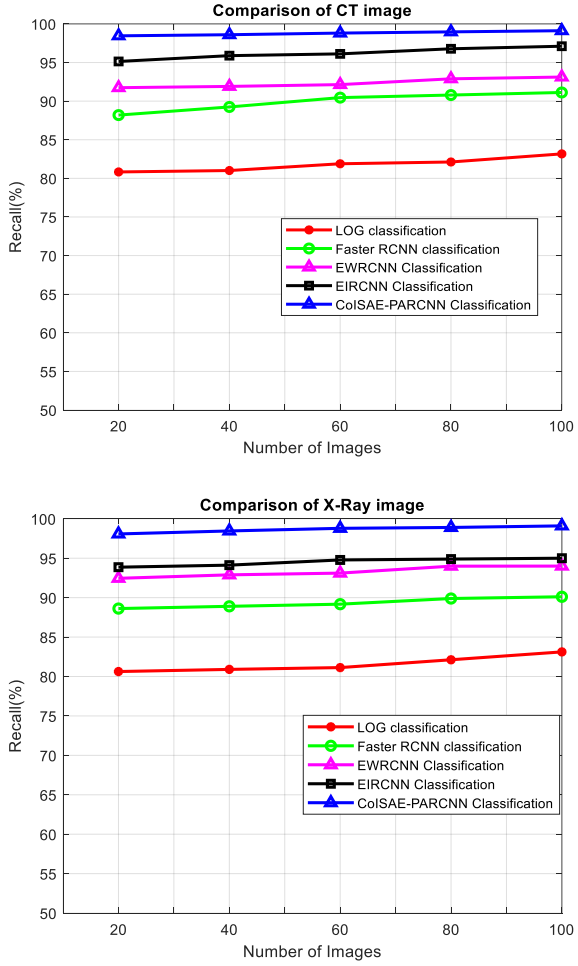

Fig.6. Recall performance comparison in various compression techniques

Fig. 6 compares Recall rates obtained by the proposed CoISAE-PARCNN, and existing LOG, Fast-RCNN, EWRCNN and EIRCNN methods. From the graphs, the proposed approach proves to be efficient for procuring 98.19% and 98.49% of Recall rate for CT and X-ray images respectively in contrast to other prevailing methods RCNN, Faster RCNN, EWRCNN and

EIRCNN solely obtain low rate of recall ratios. It represents that the proposed CoISAE-PARCNN is efficient for optimal detection rate. By having the efficient stage of image enhancement and ISAEDNN based feature extraction, the proposed method becomes effective, through which it diminishes the noise with the help of NSCT.

Accuracy Result Comparison

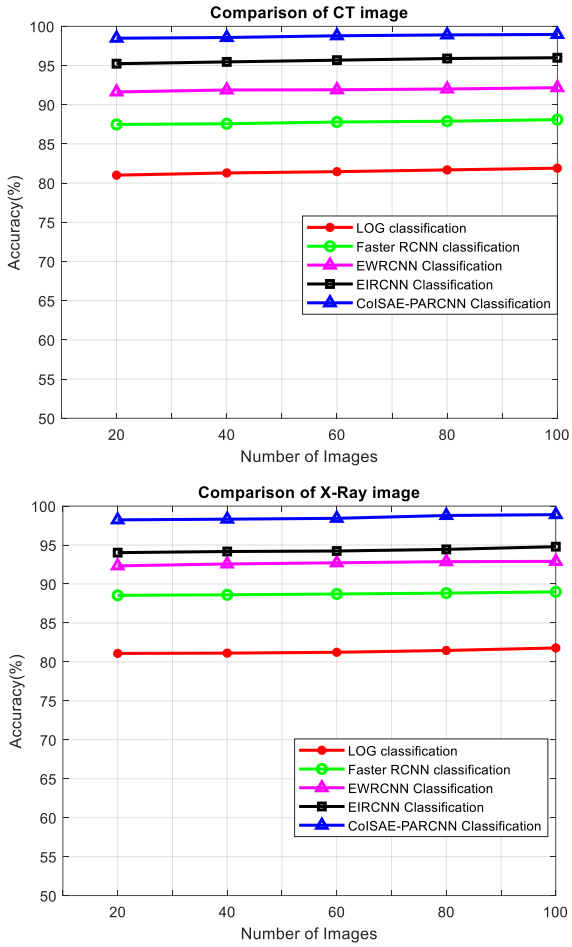

Fig.7. Accuracy performance comparison in various compression techniques

In Fig. 7, accuracy values obtained by the proposed CoISAE-PARCNN, and existing LOG, Fast-RCNN, EWRCNN and EIRCNN methods have compared. From the graphs, the proposed approach proves to be effective than other prevailing methods, as the proposed CoISAE-PARCNN approach secures 98.25% and 98.60%of the accuracy for CT and X-ray respectively. Whereas, other prevailing approaches, such as RCNN, Faster RCNN, EWRCNN and EIRCNN solely attain low accuracy for both CT and X-ray images. Moreover, the reason for the efficiency of the proposed method is that the pre-activation mechanism that carries feature recalibration adaptively and learn more robust feature representations with respect to selected features from IWD and thus improves the lung nodule detection accuracy.

3.4.Error rate Result Comparison

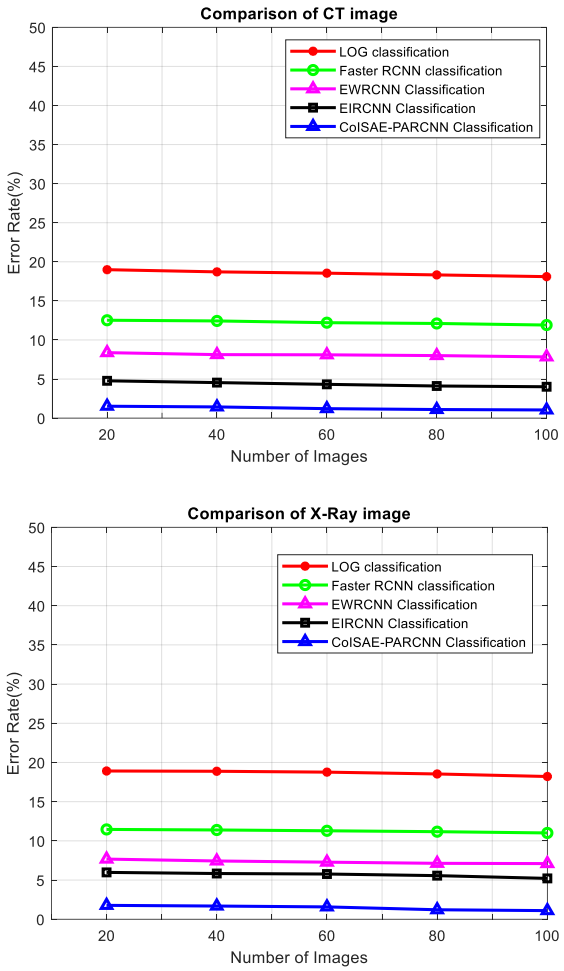

Fig.6. Error rate performance comparison in various compression techniques

Fig. 6 compares Error rate rates obtained by the proposed CoISAE-PARCNN, and existing LOG, Fast-RCNN, EWRCNN and EIRCNN methods. From the graphs, the proposed approach proves to be efficient for procuring 1.74% and 1.39% of Error rate for CT and X-ray images respectively in contrast to other prevailing methods RCNN, Faster RCNN, EWRCNN and EIRCNN solely obtain high error rate ratios. It represents that the proposed CoISAE-PARCNN is efficient for optimal detection rate for lung nodule detection.The reason is that a method of deep learning, such as stacked Auto-encoder (SAE) network, is utilized to reduce the dimensionality of the feature sets and gain the latent features which reduces the error rate at the training and testing stage of the proposed classifier.

3.5.Time Result Comparison

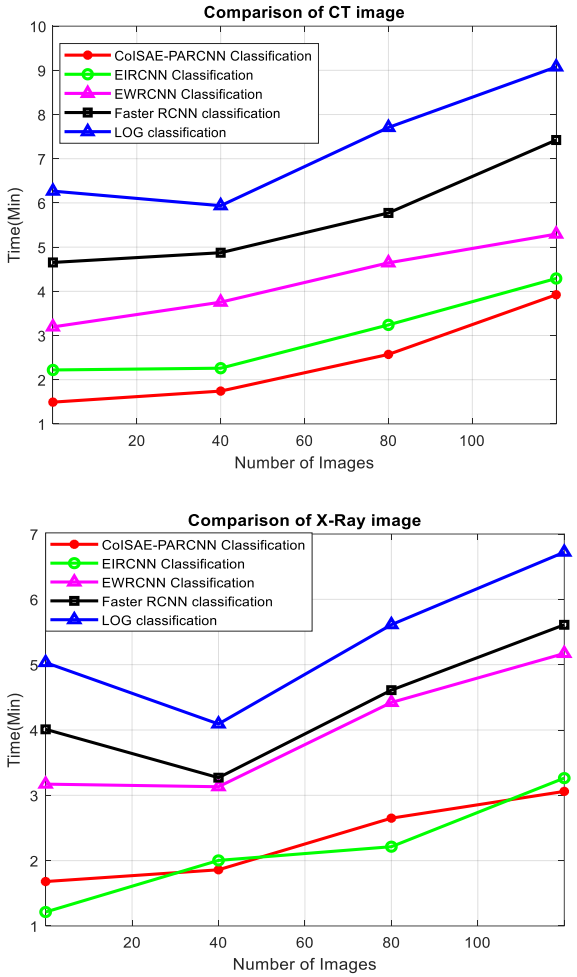

Fig.6. Time performance comparison in various compression techniques

Fig. 6 compares time obtained by the proposed CoISAE-PARCNN, and existing LOG, Fast-RCNN, EWRCNN and EIRCNN methods. From the graphs, the proposed approach proves to be efficient for procuring 1.63m and 1.98m of time rate for CT and X-ray images respectively in contrast to other prevailing methods RCNN, Faster RCNN, EWRCNN and EIRCNN solely obtain high rate of time. It represents that the proposed CoISAE-PARCNN is efficient for lung nodule detection.The reason is that in proposed model, SIPCNN can effectively capture high-level semantic concepts and project them back into the image space to generate five gray intensities with great practical value that has the ability to locate and segment the target lung nodules from the CT and X-ray image and thus reduce the computation time of the proposed classifier.

3.6.PSNR Result Comparison

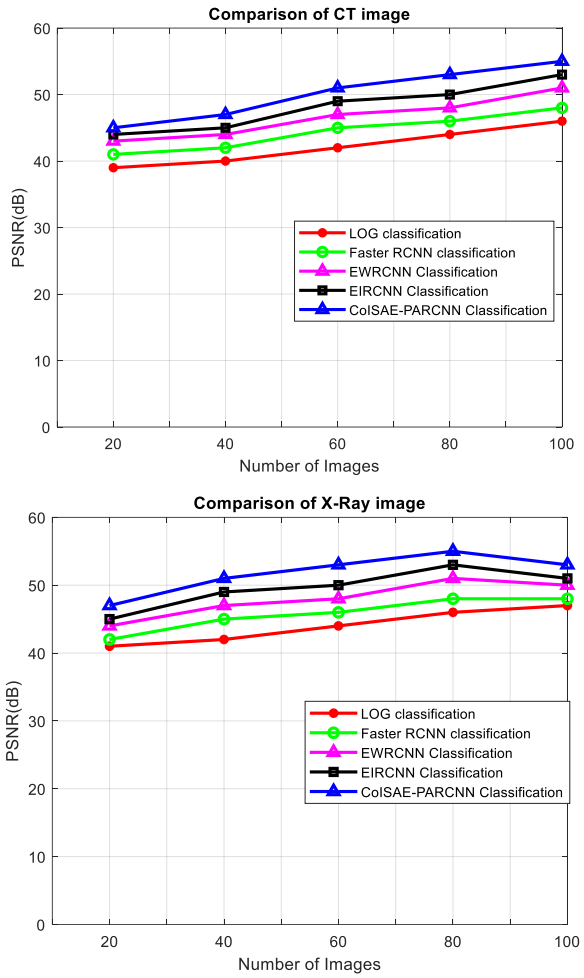

Fig.6. PSNR performance comparison in various compression techniques

Fig. 6 compares PSNR rates obtained by the proposed CoISAE-PARCNN, and existing LOG, Fast-RCNN, EWRCNN and EIRCNN methods. From the graphs, the proposed approach proves to be efficient for procuring 47dB and 45dB of PSNR rate for CT and X-ray images respectively in contrast to other prevailing methods RCNN, Faster RCNN, EWRCNN and EIRCNN solely obtain low rate of PSNR ratios. It represents that the proposed CoISAE-PARCNN is efficient for lung nodule detection. The reason is that the proposed model developed with the aim to determine the maximum entropy value in the Fuzzy set theory for brightness of grey levels in CT and X-ray images. Besides, the research focuses on evaluating the fusion approach of NGCCLAHE-based image enhancement method with Fuzzy set theory so that it can increase the contrast and brightness in CT and X-ray images and thus it improves the quality of contrast and brightness for field images and enhance the quality of the images with high PSNR.

4. Conclusion and Future work

Throughout this research work, an innovative image enhancement methodology has introduced, namely Fuzzy Normalized Gamma-Corrected Contrast-Limited Adaptive Histogram Equalization (FNGCCLAHE) with Nonsubsampled Contourlet Transform (NSCT). Through utilizing this FNGCCLAHE-NSCT, the contrast of lung nodule image is enhanced initially.

Subsequently, after FNGCCLAHE, the lung image decomposition into NSCT domain is done through low-frequency sub-band and numerous high-frequency sub-bands. Further involved a new segmentation approach, namely Sub-Intensity Range based Pulse-Coupled Neural Network (SIPCNN) for acquiring optimum segmentation results from medical Lung CT and X-ray images. Ultimately, proposed a novel deep learning model on the basis of Combined Improved Stacked Auto Encoder Deep Neural Network (ISAE-DNN) and Enhanced Pre-Activation Residual Convolutional Neural Network (EPARCNN) to carry out tumor recognition, during which the model jointly learn the feature representation, and execute the recognition, termed as (CoISAE-PARCNN). During the process of ISAE-DNN, feature extraction is done through three hidden layers, and then, classification took place using EPARCNN classifier. At this point, particle Swarm Optimization is involved to perform the feature reduction. Empirical findings depict the efficiency of the designed CoISAE-PARCNN network and the FP reduction strategy to implement the lung nodule detection in addition to FP reduction for CT and X-ray images with accuracy value of 98.25% and 98.60% respectively that accommodate accurate results.

References

1. Bjerager M., Palshof T., Dahl R., Vedsted P., Olesen F. Delay in diagnosis of lung cancer in general practice. Br. J. Gen. Pract. 2006;56:863–868.
2. Nair M., Sandhu S.S., Sharma A.K. Cancer molecular markers: A guide to cancer detection and management. Semin. Cancer Biol. 2018;52:39–55. doi: 10.1016/j.semcancer.2018.02.002.
3. Silvestri G.A., Tanner N.T., Kearney P., Vachani A., Massion P.P., Porter A., Springmeyer S.C., Fang K.C., Midthun D., Mazzone P.J. Assessment of plasma proteomics biomarker's ability to distinguish benign from malignant lung nodules: Results of the PANOPTIC (Pulmonary Nodule Plasma Proteomic Classifier) trial. Chest. 2018;154:491–500. doi: 10.1016/j.chest.2018.02.012.
4. Shi Z., Zhao J., Han X., Pei B., Ji G., Qiang Y. A new method of detecting pulmonary nodules with PET/CT based on an improved watershed algorithm. PLoS ONE. 2015;10:e0123694.
5. Available from: http://www.globocan.iarc.fr/Pages/fact_sheets_cancer.aspx. [Last accessed on 2016 Feb 20]
6. M. Bergtholdt, R. Wiemker and T. Klinder, "Pulmonary Nodule Detection Using a Cascaded SVM Classifier" in Computer-Aided Diagnosis, Bellingham, WA, USA:SPIE, vol. 9785, 2015.
7. S. G. and J. P., "A fully-automated system for identification and classification of subsolid nodules in lung computed tomographic scans", *Biomed. Signal Process. Control*, vol. 53, Aug. 2019.
8. S. Ren, K. He, R. Girshick, et al., "Faster R-CNN: towards real-time object detection with region proposal networks," IEEE Trans.Pattern Anal. Mach. Intell., vol. 39, no. 6, pp. 1137-1149, 2017
9. Fan, W., Jiang, H., Ma, L., Gao, J., & Yang, H. (2018, August). A modified faster R-CNN method to improve the performance of the pulmonary nodule detection. In *Tenth International Conference on Digital Image Processing (ICDIP 2018)* (Vol. 10806, p. 108065A). International Society for Optics and Photonics.

10. Zuo, W., Zhou, F., Li, Z., & Wang, L. (2019). Multi-resolution CNN and knowledge transfer for candidate classification in lung nodule detection. *Ieee Access*, *7*, 32510-32521.
11. Cao, H., Liu, H., Song, E., Ma, G., Xu, X., Jin, R., ... & Hung, C. C. (2020). A two-stage convolutional neural networks for lung nodule detection. *IEEE journal of biomedical and health informatics*, *24*(7), 2006-2015.
12. Ali, I., Muzammil, M., Haq, I. U., Khaliq, A. A., & Abdullah, S. (2020). Efficient Lung Nodule Classification Using Transferable Texture Convolutional Neural Network. *IEEE Access*, *8*, 175859-175870.
13. SM Pizer, RE Johnston, JP Ericksen, BC Yankaskas, KE Muller, Contrast-limitedadaptive histogram equalization: speed and effectiveness (Proceedings of theFirst Conference on Visualization in Biomedical Computing, United States,1990), pp. 337–345
14. KU Khan, J Yang, W Zhang, Unsupervised classification of polarimetric SARimages by gamma-correction of features using self organizing map. ChineseJ Electron. 18(4), 767–770 (2009)
15. RC Gonzalez, RE Woods, Digital image processing, 3rd edn. (Prentice Hall,New Jersey, 2007). pp. 132–135
16. S Vimal, P Thiruvikraman, Automated image enhancement using power lawtransformations. Sadhana-Acad P Eng S. 37(6), 739–745 (2012)
17. R Arun, MS Nair, R Vrinthavani, R Tatavarti, An alpha rooting based hybridtechnique for image enhancement. Eng Let. 19(3), 1–10 (2011)
18. CM Tsai, Adaptive local power-law transformation for colorimageenhancement. Appl Math Inform Sci. 7(5), 2019–2026 (2013)
19. A Khunteta, D Ghosh, Fuzzy rule-based image exposure level estimation andadaptive gamma correction for contrast enhancement in dark images (11th IEEEInternational Conference on Signal Processing, China, 2012), pp. 667–672
20. R Boss, K Thangavel, D Daniel, Automatic mammogram image breast regionextraction and removal of pectoral muscle. Int J Sci Eng Res.4(5), 1722–1729 (2013)
21. A Reza, Realization of the contrast limited adaptive histogram equalization (CLAHE)for real-time image enhancement. J VLSI Sig Proc Syst. 38(1), 35–44 (2004)
22. V Schatz, Low-latency histogram equalization for infrared image sequences:a hardware implementation. J. Real-Time Image Proc. 8(2), 193–206 (2013)
23. Yang, Z., Lian, J., Li, S., Guo, Y., Qi, Y., & Ma, Y. (2018). Heterogeneous SPCNN and its application in image segmentation. Neurocomputing, 285, 196-203.
24. Y.chen,S>K.Park, Y.MA,R.Ala, a new automatic parameter setting method of a simplified PCNN for image segmentation.IEEE trans,Neural.Netw.22(2011)880-892.
25. J.Lian,B.shi, M.Li, Z.Nan, Y.Ma, An automatic segmentation method of s prameteradptive PCNN for medical images, Int.J.Comput.Assist.Radiol.Surg.12(2017)1-9.
26. J. Donahue, L. A. Hendricks, S. Guadarrama, M. Rohrbach, S. Venugopalan, K. Saenko, and T. Darrell. Long-term recurrent convolutionalnetworks for visual recognition and description. In CVPR, 2015.
27. Lin, Min, Qiang Chen, and Shuicheng Yan. "Network in network." arXiv preprint arXiv: 1312.4400 (2013).\

28. Iandola, Forrest N., et al. "SqueezeNet: AlexNet-level accuracy with 50x fewer parameters and< 0.5 MB model size." arXiv preprint arXiv:1602.07360 (2016).
29. Agarwal, B., & Mittal, N. (2016). Prominent feature extraction for review analysis: an empirical study. *Journal of Experimental & Theoretical Artificial Intelligence*, *28*(3), 485-498.
30. Zhan K, Zhang H, Ma Y (2009) New spiking cortical model for invariant texture retrieval and image processing. IEEE Trans on Neural Netw 20(12):1980–1986.
31. Wang, L., You, Z. H., Chen, X., Xia, S. X., Liu, F., Yan, X., ... & Song, K. J. (2018). A computational-based method for predicting drug–target interactions by using stacked autoencoder deep neural network. *Journal of Computational Biology*, *25*(3), 361-373.